Agricultural and Forest Meteorology 275 (2019) 255–264

Contents lists available at ScienceDirect

Agricultural and Forest Meteorology

journal homepage: www.elsevier.com/locate/agrformet

An evaluation of the flux-gradient and the eddy covariance method to measure CH_4, CO_2, and H_2O fluxes from small ponds

Jiayu Zhao[a,b], Mi Zhang[a,b,d], Wei Xiao[a,b,d], Wei Wang[a,b], Zhen Zhang[a,b], Zhou Yu[a,b], Qitao Xiao[a,b], Zhengda Cao[a,b], Jingzheng Xu[a,b], Xiufang Zhang[a,b], Shoudong Liu[a,b], Xuhui Lee[c,a,*]

[a] Yale-NUIST Center on Atmospheric Environment, International Joint Laboratory on Climate and Environment Change (ILCEC), Nanjing University of Information Science and Technology, Nanjing, Jiangsu Province, China
[b] Key Laboratory of Meteorological Disaster, Ministry of Education and Collaborative Innovation Center on Forecast and Evaluation of Meteorological Disasters, Nanjing University of Information Science and Technology, Nanjing, Jiangsu Province, China
[c] School of Forestry and Environmental Studies, Yale University, New Haven, CT, USA
[d] NUIST-Wuxi Research Institute, Wuxi, Jiangsu Province, China

ARTICLE INFO

Keywords:
Fish pond
Flux-gradient method
Eddy covariance method
Modified Bowen-ratio method
Methane flux
Carbon dioxide flux

ABSTRACT

Despite their small overall area, small ponds play a large role in the greenhouse gas budgets of inland water bodies. This study aims to evaluate the performance of the flux-gradient (FG) and the eddy covariance (EC) method for measuring the fluxes of CO_2, CH_4, and H_2O at two small fish ponds (fetch < 120 m) in subtropical climate conditions. The EC fluxes were subject to two sources of error: high frequency flux loss and footprint contamination. Of the three gaseous fluxes, the CH_4 flux suffered the largest high frequency loss (18%) due to a combination of low EC instrument height and long optical path of the CH_4 analyzer. Despite the low measurement height, the EC fluxes were influenced by sources outside the boundary of the target fish ponds, with the footprint contamination most severe on the CO_2 flux and least severe on the CH_4 flux. With regards to the FG method, one major uncertainty lies in the eddy diffusivity calculation. Of the three eddy diffusivity models evaluated [the aerodynamic (AE) model deploying the full Obukhov stability correction, the modified Bowen-ratio model using H_2O as a tracer, and the wind profile model for neutral stability], the AE model yielded the best results for the CO_2 and CH_4 fluxes. Our results support Horst's (1999, Boundary-Layer Meteorology 90, 171) theoretical prediction that the footprint of the AE flux based on a two-level concentration profile measurement should be much smaller than that of the gradient flux footprint and the EC flux footprint at the geometric mean of the two heights. We conclude that the most appropriate micrometeorological method for measuring fluxes from small water bodies is a hybrid scheme, whereby an EC system is deployed to measure the eddy diffusivity and a precision gas analyzer is used to obtain the concentration gradient of the target gas.

1. Introduction

Small ponds (area smaller than about 0.01 km^2) comprise over 90% of all inland water bodies in terms of numbers (Downing et al., 2006; Verpoorter et al., 2014). They are increasingly recognized as hotspots of CO_2 (Abnizova et al., 2012; Catalán et al., 2014), CH_4 (Holgerson, 2015; Wik et al., 2016; Yuan et al., 2019), and N_2O emission (Williams and Crutzen, 2010; Hu et al., 2012) in inland waters. According to Holgerson and Raymond (2016), despite occupying less than 8.6% of the total water surface area, very small ponds (area smaller 0.001 km^2) contribute disproportionately 15% of the total CO_2 emission and 40% of the total CH_4 emission from inland waters. Currently large uncertainties exist in these estimates. For example, in the meta analysis by Holgerson and Raymond (2016), the uncertainty (standard error) of the CH_4 emission from small ponds is on the order of 30%. These uncertainties are not only related to the uncertainty of the area, number and spatial distribution of small ponds but also related to the sparsity of the actual flux observations (Jonsson et al., 2008). More flux measurements at small ponds are needed in order to reduce these uncertainties and to improve our understanding of the role of aquatic ecosystems in the global greenhouse gas cycles.

Greenhouse gas fluxes of small ponds are traditionally measured with flux chambers (Catalán et al., 2014; Natchimuthu et al., 2014; Liu et al., 2015) and the water equilibrium method (Abnizova et al., 2012; Schubert et al., 2012; Xiao et al., 2014a; Holgerson, 2015). The chamber method determines the flux by monitoring the accumulation

* Corresponding author at: School of Forestry and Environmental Studies, Yale University, New Haven, CT, USA.
E-mail address: xuhui.lee@yale.edu (X. Lee).

https://doi.org/10.1016/j.agrformet.2019.05.032
Received 6 March 2019; Received in revised form 23 May 2019; Accepted 29 May 2019

of the target gas over time in an enclosure, whose dimensions are typically smaller than 1 m, floating on the water surface. The water equilibrium method calculates the flux using a piston velocity and the concentration of the gas in the water, the latter of which is determined from the concentration in air that is brought to equilibrium with the water taken from a point in the pond. Due to their simplicity and relatively inexpensive nature, these methods have been widely used in past studies (Cole and Caraco, 1998; Huttunen et al., 2003; Cole et al., 2010). However, they cannot be used continuously over long periods of time (weeks to months). For this reason, the dynamics of the fluxes may be missed across multiple temporal scales, especially at hourly and daily scales. Because of their microscale nature, these measurements may be subject to large uncertainties if the flux is spatially variable. Furthermore, the water equilibrium method cannot capture the CH_4 ebullition signal, which is a significant component of the overall CH_4 emission in small lakes and ponds (Schubert et al., 2012; DelSontro et al., 2016). Finally, neither method can measure the flux of water vapor. Although water vapor flux itself is not a component of the greenhouse gas cycling in the environment, its measurement can elucidate site-level understanding of drivers of the greenhouse gas fluxes.

The micrometeorological eddy covariance (EC) and flux-gradient (FG) method can overcome the above limitations (e.g., Swinbank, 1951; Monteith and Szeicz, 1960; Baldocchi et al., 1988). For example, these two methods are not sensitive to microscale spatial variations in the flux because the measured flux has a relatively large footprint on the order of tens of meters. However, this advantage actually becomes a challenge in an experiment involving a small water body because the flux footprint can extend beyond the water boundary. A low observation height may be necessary to reduce the flux footprint and the contamination from gaseous sources outside the water body. Application of the EC method is often limited by the need to correct for high-frequency flux loss (Moore, 1986). It is known that the eddies contributing to scalar and momentum transports become smaller at a lower height above the surface (Kaimal and Finnigan, 1994). By lowering the instrument height, the high-frequency loss will become more significant. High-frequency loss is especially a concern for EC systems that use trace analyzers with a long optical path, such as the LI-7700 open-path CH_4 analyzer.

In comparison, the FG method is not affected by the high frequency loss, and in theory its measurement heights can be made very close to the surface to avoid footprint contamination. Another advantage of the FG method, which is usually equipped with a closed-path sensor, over the EC method is that it avoids the density effects due to temperature variations (Webb et al., 1980) and is therefore unaffected by errors that may propagate through the density correction procedure. Error propagation is a large source of uncertainties concerning small flux signals measured with EC, such as the CO_2 flux of natural waters (Lee, 2018). The FG method, which determines the gas fluxes by multiplying the vertical gas concentration gradients with an eddy diffusivity, has been used for studies of greenhouse gas fluxes over a large lake (Xiao et al., 2014b), an extensive rice paddy (Simpson et al., 1995), and a wide river (Zappa et al., 2003). We are not aware of an FG application for small ponds. It is not known how low is low enough for the measurement intakes to ensure accurate flux determination.

A challenge of the FG method is eddy diffusivity parameterization. The aerodynamic (AE) model calculates the eddy diffusivity on the basis of the Monin-Obukhov similarity theory. One difficulty of the AE model is that it requires accurate measurements of the friction velocity (u_*) and sensible heat flux for evaluating the Obukhov stability function; These are typically obtained using an EC system. Alternatively, the eddy diffusivity can be determined with the modified Bowen-Ratio (MBR) model without the need for stability correction (Businger, 1986; Meyers et al., 1996). The MBR method requires simultaneous measurements of the concentration gradient and the flux of another gas (typically water vapor) and the assumption that the eddy diffusivity is identical between this gas and the target gas. A third option, referred to as the wind profile (WP) model here, is to calculate the eddy diffusivity using the wind speed measurement only and assuming neutral stability. The assumption of neutral stability may be acceptable because mechanical generation of turbulence is much stronger than buoyancy generation very close to the surface and because sensible heat flux is typically small over a water body. The WP model can be used in situations where fast-response instruments are not available for measuring the friction velocity or the water vapor flux.

In this study, we measured the fluxes of water vapor, carbon dioxide, and methane with the FG and the EC method at two small subtropical fish ponds in China. Our specific goals are: (1) to quantify high-frequency flux loss associated with the EC method, (2) to assess the applicability of the FG method using the three eddy diffusivity models, and (3) to compare the different extents of footprint contamination among the EC and FG fluxes of the three gases.

2. Methods

2.1. Study site

The study site was located in the Guandu International Observatory of Yale-NUIST (Nanjing University of Information, Science and Technology) Center on Atmospheric Environment (31° 58′ N, 118° 15′ E, Fig. 1), in Anhui Province, China. The mean air temperature is 15.8 °C and the mean annual precipitation is 1090 mm from 1980 to 2016. The target surface was two small fish ponds, each about the size of 110 m by 60 m (Ponds D and F, Fig. 1). The data were collected from two periods, Period 1 from March 24 to March 31, 2016 and Period 2 from October 20 to November 5, 2016, when the EC and the FG measurements were made simultaneously. Ponds D and F were dry in Period 1 and was filled with water to a depth of 0.8 m during Period 2 for the purpose of raising Chinese Carps. Lush lotus plants grew in Pond B that was filled with water and neighbored Pond D. To the northeast of Pond D and F were rice paddies. The other three ponds (A, C and E) were fish ponds with a water depth of about 1.5 m in both measurement periods. The mean air temperature was 12.3 °C and 14.7 °C for Periods 1 and 2, respectively. The acceptable wind direction range was 28°–95° (Fig. 1). In this wind direction range, the measurement was not influenced by the instrument mast.

2.2. Instrumentation

The EC system consisted of a three-dimensional sonic anemometer/thermometer (model CSAT3A, Campbell Scientific Inc., Logan, Utah,

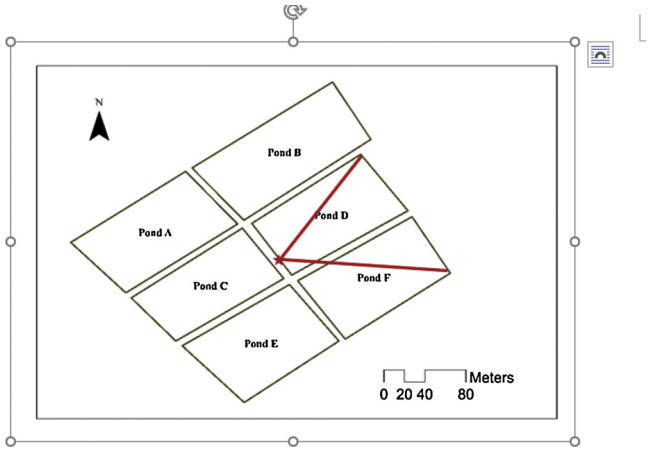

Fig. 1. Map showing the target ponds (Ponds D and F), measurement location (marked by the star) and the acceptable wind direction range (red lines). (For interpretation of the references to colour in this figure legend, the reader is referred to the web version of this article).

USA), an open-path CO_2/H_2O infrared gas analyzer (model EC150, Campbell Scientific Inc.), and an open-path CH_4 gas analyzer (model LI-7700, LI-COR Inc., Lincoln, Nebraska, USA). The EC system was directed to a northeasterly direction (40°), which was the prevailing wind direction of our study site. The raw 10 Hz data were saved by a data logger (model CR3000, Campbell Scientific Inc.) for offline flux calculation. The measurement height, referenced to the bottom of Pond D, was 2.8 m. So the effective measurement height was 2.8 m in Period 1 and 2.0 m in Period 2.

The FG gas intakes were installed approximately 2.0 m away from the EC sensors at heights of 3.0 m and 1.7 m above the bottom of Pond D. The effective geometric mean height was 2.3 m in Period 1 and 1.4 m in Period 2. The FG system was set up similarly to that of a previous study which deployed the FG technique to measure the H_2O, CO_2, and CH_4 fluxes at a large lake (Xiao et al., 2014b). A high-resolution fast OA-ICOS (Off-Axis Integrated-Cavity Output Spectroscopy) analyzer (model 915-0011-CUSTOM, Los Gatos Research Ltd., San Jose, California, USA) was employed to measure the mixing ratios of CO_2, H_2O, and CH_4 at 1 Hz. The 100-s precision of the analyzer is 0.040 ppm for CO_2, 0.250 ppb for CH_4, and 0.0015%v for H_2O according to the manufacturer. Air was continuously drawn from the two air intakes above the water surface through Teflon tubings (length 4 m; tube inner diameter, 0.32 cm) into two buffer bottles (volume 4 L). The analyzer was commanded to sample, in an alternate fashion, the two air flows downstream of the buffers. Each sampling cycle was 2 min. The sampling tubes were heated by a self-regulating heating tape to about 5 °C above the environmental temperature to prevent condensation in the tubes. The raw 1 Hz data were averaged to 30-min mean values for the upper and lower inlets. (The data collected in the first 25 s after each inlet switching were discarded from the averaging.) The analyzer was calibrated before each field experiment period to ensure measurement accuracy. A zero-gradient test, during which both inlets were positioned at the same point above the pond, was used to check the measurement biases of the FG system. The test results indicate a small measurement bias (lower inlet reading minus upper inlet reading; mean value ± one standard deviation) of -0.070 ± 0.107 ppm for CO_2, -0.023 ± 0.102 ppb for CH_4, and 0.0004 ± 0.0005%v for water vapor, which is equivalent to a flux uncertainty of -0.010 ± 0.016 mg m^{-2} s^{-1} for CO_2, -0.001 ± 0.005 μg m^{-2} s^{-1} for CH_4, and 0.52 ± 0.83 W m^{-2} for water vapor at a typical eddy diffusivity of 0.10 m^2 s^{-1}.

2.3. Data processing

2.3.1. Flux-gradient data

The flux-gradient method is expressed as

$$F = c\rho_a K \frac{r_1 - r_2}{z_1 - z_2} \quad (1)$$

where F is the flux of CO_2, CH_4 or H_2O, z_1 and z_2 represent the lower and upper air intake height, r_1 and r_2 are the dry molar mixing ratio at the height of z_1 and z_2, respectively, ρ_a is air density, c is the unit conversion constant (for conversion from molar to mass mixing ratio), and K is the eddy diffusivity. For this study, we use the following mass flux units for the two greenhouse gases: mg m^{-2} s^{-1} for CO_2 and μg m^{-2} s^{-1} for CH_4. For H_2O, the flux is expressed as latent heat flux in W m^{-2}. Use of the dry mixing ratios eliminated the density effects associated with water vapor fluctuations. The eddy diffusivity was determined with three methods as described below.

According to the aerodynamic model, the eddy diffusivity is given as:

$$K = ku_* z_g/\varphi_h \quad (2)$$

where k = 0.4 is von Kármán constant, u_* is the friction velocity, measured by the sonic anemometer, z_g is the geometric mean of upper and lower air intakes heights, and φ_h represents the Obukhov stability function for heat given by Dyer and Hicks (1970).

The MBR model expresses the flux as

$$F_2 = F_1 \frac{\Delta C_2}{\Delta C_1} \quad (3)$$

where ΔC is the mass mixing ratio difference between the upper and lower intake, subscript 1 denotes H_2O and subscript 2 denotes CO_2 or CH_4. In this study, we used water vapor as the tracer, and the target measurement gases were CO_2 and CH_4. An implicit assumption of the MBR model is that the eddy diffusivity, estimated by dividing the water vapor flux with the H_2O concentration gradient, can be used to determine the flux of the target gases.

The WP model is a special case of the aerodynamic approach. In neutral stability, the friction velocity and the eddy diffusivity are given by

$$u_* = k\,\bar{u}/\ln\frac{z}{z_o} \quad (4)$$

$$K = k\,u_* z_g \quad (5)$$

where z is the height of the wind speed measurement, $\bar{u}$ is the mean wind speed at height z provided by sonic anemometer, and z_o is the momentum roughness. Eliminating u_* from Eqs. (4) and (5), we obtain,

$$K = k^2 z_g \bar{u}/\ln\frac{z}{z_o} \quad (6)$$

An assumption implicit in the WP model is that the eddy diffusivity for momentum transfer is equal to those for scalars. The surface roughness is usually determined from the wind speed profile measured with cup or 2-D sonic anemometers at two or more heights (Monteith and Unsworth, 1990). Here, the z_o value was obtained by linear regression of the friction velocity against the mean wind speed, both measured by the EC system. The slope of the regression according to Eq. (4) is 0.112 and 0.073 for when Ponds D and F were dry and when they were filled with water, respectively, from which the z_o can then be determined. This procedure yielded a z_o value of 0.078 m for Period 1 and 0.0083 m for Period 2. These z_o values were used for the K calculation with Eq. (6) and also for the footprint analysis described below.

2.3.2. EC data processing

The post-processing software EddyPro (version 6.2.1, LI-COR Inc.) was used to calculate 30-min EC CO_2, H_2O, and CH_4 fluxes. Briefly, the raw data was firstly checked against a series of data quality control criteria, including spike detection, amplitude resolution, dropout, absolute limit, and skewness and kurtosis, using the default threshold values in the software. Time lags were determined from the cross-covariance maximum function. A double coordinate rotation was applied (e.g., Tanner and Thurtell, 1969; Lee et al., 2004). Corrections for the density fluctuations caused by heat and water vapor were made to the CO_2, H_2O, and CH_4 fluxes according to the WPL procedure (Webb et al., 1980). The spectroscopic effects of pressure, temperature, and water vapor fluctuations on the CH_4 flux were removed using the method reported by McDermitt et al. (2011) and imbedded in the Eddypro software. A small spectroscopic effect on the CO_2 flux associated with the EC150 analyzer was corrected following the method described by Helbig et al. (2016). In this study, we also applied a frequency response correction to account for the EC flux loss at high frequencies caused by sensor separation and path-length averaging (Moncrieff et al., 1997).

The EC data quality was determined according to the steady-state test and the integral turbulence test. The EC data quality flag was divided into three classes and expressed as 0 (best quality), 1 (good quality), and 2 (bad quality). In this study, data that satisfied quality classes 0 and 1 were selected to compare with the FG results.

2.4. Footprint analysis

In this study, the flux footprint model of Kljun et al. (2015) was used to investigate the contribution from the target ponds to the measured fluxes. This model provides a two-dimensional footprint function spanning a range of atmospheric conditions and measurement heights. The main input variables include measurement height, roughness length, friction velocity (u_*), the Obukhov length, the standard deviation of the cross-wind component, wind direction, mean wind speed, and the boundary layer height. Apart from the boundary layer height, other parameters were measured by the EC system. The boundary layer height was provided by the Global Data Assimilation System of the U.S. National Oceanic and Atmospheric Administration (https://ready.arl.noaa.gov/gdas1.php). The grid point used was centered at 31° 58′ N, 118° 15′ E and the original 3 -hourly values were linearly interpolated to half-hourly values for the footprint calculation. In the case of the EC footprint, the measurement height was the EC instrument height (z = 2.8 m for Period 1 and 2.0 m for Period 2). In the case of the FG footprint, the measurement height was set to the geometric mean height (2.3 m and 1.4 m for Periods 1 and 2, respectively).

Horst (1999) showed that if the flux is computed from a two-level profile measurement, as in the present study, its footprint distribution, termed the "profile footprint", is different from that of the direct eddy covariance measurement ("direct footprint") and that of the concentration gradient at the geometric mean height ("gradient footprint"). Unlike the Kljun model, the Horst model computes only the footprint distribution in the along-wind direction. Here we used the Horst model to compute the three 1D footprint functions – profile, gradient, and direct – for our instrument configurations and under neutral stability. One drawback of the Horst model is that the cumulative footprint contribution does not converge to unity, a problem noted by Kormann and Meixner (2001) and Lee (2018). To ensure proper comparison, the three footprint functions were re-scaled so that their cumulative values all converged to unity at large fetches.

3. Results and discussion

3.1. High-frequency corrections to the EC fluxes

As mentioned in the introduction, low observation heights of the EC system may result in large loss of fluxes at high frequencies. Here we performed a co-spectral analysis on CH_4, CO_2, and H_2O. In this analysis, we selected raw 10 Hz data from five 30-min observations from each of the two observational periods, computed the co-spectra for each observation, and averaged among the observations to give the composite co-spectra shown in Fig. 2. The co-spectral model of Kaimal model (Kaimal et al., 1972) is also shown for comparison. An ideal case is that the gas concentration-vertical velocity co-spectrum follows the temperature-vertical velocity co-spectrum and the Kaimal model. The CO_2 and H_2O co-spectra seemed to fit this ideal characterization (Fig. 2a & c), suggesting only small flux losses at high frequencies. The normalized CH_4 flux co-spectrum was lower than the Kaimal co-spectrum at normalized frequencies greater than 0.11 in Period 1 (Fig. 2b) and 1.5 in Period 2 (Fig. 2d).

The cumulative frequency loss was assessed with the EddyPro software. With the frequency correction turned on, the H_2O flux was 8% higher, and the measured CO_2 flux was 14% lower in magnitude than the flux with the correction turned off (Supplementary Fig. S1 a & b). The CH_4 with the frequency correction was 18% greater than the CH_4 flux without the correction (Supplementary Fig. S1c). The larger frequency loss for CH_4 than for CO_2 and H_2O can be explained by the longer optical path of the CH_4 analyzer (0.47 m) than that of the CO_2/H_2O analyzer (0.15 m). In the following, the EC fluxes were corrected for these frequency losses.

Wolf et al. (2008) reported a slightly higher frequency correction of 15%–18% to their CO_2 and H_2O fluxes than our correction amounts. Their EC system deployed a different type of analyzer (model LI-7500, LI-COR Inc.), and at a lower measurement height of 1.3 m than ours (2.8 m in Period 1 and 2.0 m in Period 2). Additionally, the separation distance between their LI-7500 analyzer and sonic anemometer (10–20 cm) was greater than the separation distance (5 cm) in the present study. In another related study, McDermitt et al. (2011) found negligible frequency loss in the CH_4 flux co-spectrum measured with a LI-7700 gas analyzer. Their measurement height of 1.9 m was similar to ours, but their underlying surface, an arctic tundra wetland, was rougher than ours. Plant canopies are known to generate large coherent eddies through the shear instability mechanism (Kaimal and Finnigan, 1994), and so the role of small eddies becomes weakened.

3.2. Comparison between the eddy covariance and the flux-gradient method

3.2.1. Latent heat flux comparison

The flux obtained with the AE flux-gradient method showed similar temporal variations as the EC flux (Fig. S2). On average, the AE latent heat flux was 17% smaller than the EC flux (mean value ± one standard error: 60.2 ± 2.60 W m^{-2} for EC and 50.0 ± 2.32 W m^{-2} for AE; Table 1). In comparison, although the WP model gave a reasonable linear correlation with the EC flux (linear correlation coefficient 0.82; Fig. 3b), the mean flux obtained with the WP flux-gradient method was only 35.4 ± 1.87 W m^{-2}, or 59% of the mean EC flux.

3.2.2. CO_2 flux comparison

The EC CO_2 flux was compared with the flux obtained with the three different flux-gradient methods (AE, MBR, and WP), using scatter plots (Fig. 4), mean statistics (Table 1) and a time series plot (Fig. S3). On average, the three flux-gradient methods gave slightly more positive values (or emission flux) and smaller variations than the EC method (Table 1; Fig. S3). The best agreement was achieved between the MBR and the EC method in terms of linear correlation coefficient (0.64) and linear regression slope (0.91; Fig. 4a).

A previous study over a lake surface also found a larger scatter for the EC CO_2 flux than for the flux obtained with the AE flux-gradient method (Xiao et al., 2014b). The comparison here shows that the AE CO_2 goes to zero when the EC flux is negative. The negative EC flux (as negative as -0.15 mg m^{-2} s^{-1}) is generally larger in magnitude than the detection limit of the FG system (-0.010 ± 0.016 mg m^{-2} s^{-1}), so factors other than the FG detection limit may have contributed to the observed scatter. One contributor may be related to error propagation through open-path CO_2 flux density correction terms. Another more likely cause of the large scatter was contamination of the EC CO_2 flux signal by photosynthesis and respiration of the plants growing around the target ponds (Section 3.4).

3.2.3. CH_4 flux comparison

The CH_4 flux measured with the EC method and the AE flux-gradient method compared favorably (Figs. 5b, S4), with a linear correlation of 0.84 and the mean value of 1.31 ± 0.093 μg m^{-2} s^{-1} for EC and 1.34 ± 0.107 μg m^{-2} s^{-1} for AE for the two periods. The MBR method also showed good correlation with the EC method (r = 0.86, Fig. 5a), but its mean value (1.66 ± 0.129 μg m^{-2} s^{-1}) was 27% higher than the EC mean value (Table 1). The CH_4 flux determined with the WP model was significantly lower than that from the EC CH_4 measurement, amounting to a mean underestimation of 20% (Fig. 5c).

The overall good agreement between the EC flux and the AE flux validated the high frequency correction made by the EddyPro software. Without this correction, the mean EC CH_4 flux would be 1.11 ± 0.075 μg m^{-2} s^{-1}, which is 17% lower than the mean flux obtained from the AE method.

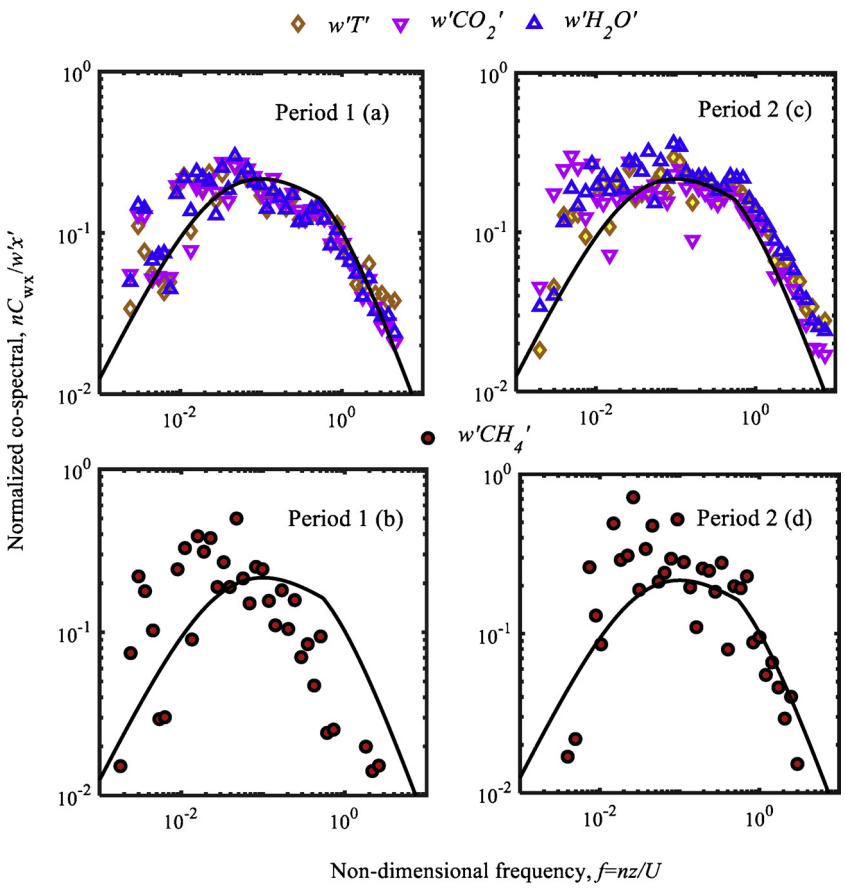

Fig. 2. Ensemble averaged co-spectra for Period 1(a, b) and Period 2 (c, d). The ideal curve (black line) represents the Kaimal model.

Table 1
Mean value (± one standard error) of CH_4, CO_2 and latent heat flux during the Period 1 and Period 2.

Method	Period 1	Period 2	All data
		CH_4 flux (μg m^{-2} s^{-1})	
EC	0.92 (± 0.094)	1.39 (± 0.109)	1.31 (± 0.093)
AE	1.25 (± 0.158)	1.36 (± 0.125)	1.34 (± 0.107)
MBR	1.71 (± 0.155)	1.66 (± 0.152)	1.66 (± 0.129)
WP	1.42 (± 0.212)	0.98 (± 0.129)	1.05 (± 0.113)
		CO_2 flux (mg m^{-2} s^{-1})	
EC	0.098 (± 0.019)	−0.006 (± 0.004)	0.011 (± 0.006)
AE	0.104 (± 0.014)	0.006 (± 0.001)	0.022 (± 0.004)
MBR	0.111 (± 0.021)	0.007 (± 0.002)	0.024 (± 0.005)
WP	0.120 (± 0.018)	0.004 (± 0.001)	0.023 (± 0.005)
		Latent heat flux (W m^{-2})	
EC	43.3 (± 6.10)	65.2 (± 2.69)	60.2 (± 2.60)
AE	30.2 (± 4.48)	55.9 (± 2.47)	50.0 (± 2.32)
WP	26.2 (± 3.31)	38.1 (± 2.16)	35.4 (± 1.87)

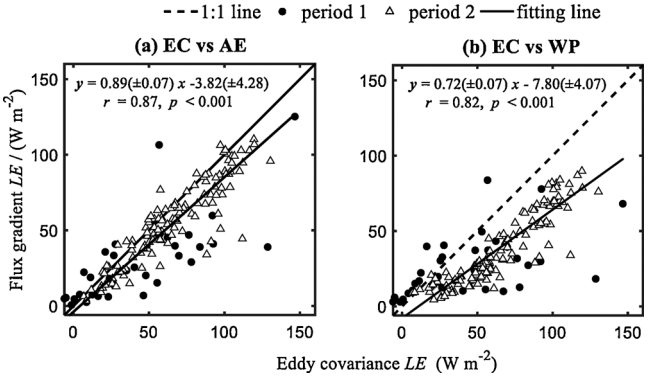

Fig. 3. Comparison of latent heat flux measured with the flux-gradient method and the eddy-covariance method. Also shown are regression equation, linear correlation (r) and significance (p). Parameter bounds on the regression coefficients are 95% confidence intervals.

3.3. Comparison of the three eddy diffusivity models

3.3.1. Mean differences

Since all the three FG methods used the same gradient data, the differences in the fluxes originated from differences in the eddy diffusivity calculated or implied by these methods. Although it does not involve directly the eddy diffusivity calculation, the MBR method implies that the eddy diffusivity for water vapor can be used for CO_2 and CH_4. For the diagnostic purpose, we computed this diffusivity by inverting Eq. (1), where $\Delta r/\Delta z$ is water vapor mixing ratio gradient and F is water vapor flux. The MBR K was 43% and 24% greater than the K derived from the AE method for Period 1 and Period 2, respectively (Table 2). Unsurprisingly, the MBR CH_4 flux was higher by the similar relative amounts (37% and 22%) in comparison to the AE flux (Table 1). The WP method produced the lowest eddy diffusivity values among the three models (Table 2), which is consistent with the low fluxes obtained with this method (Table 1).

3.3.2. Effects of stability and surface roughness

To help understand the causes of these differences, a comparison was made separately for three different stability classes using the Obukhov length L (Fig. 6): neutral ($|L| > 100$ m), unstable (-100 m $< L <$ 0), and stable (0 $< L <$ 100 m). With only a few exceptions, the half-hourly K from the MBR method was higher than the AE K for all three stability classes regardless of the measurement periods (Fig. 6d–f). We attributed this systematic difference to a footprint

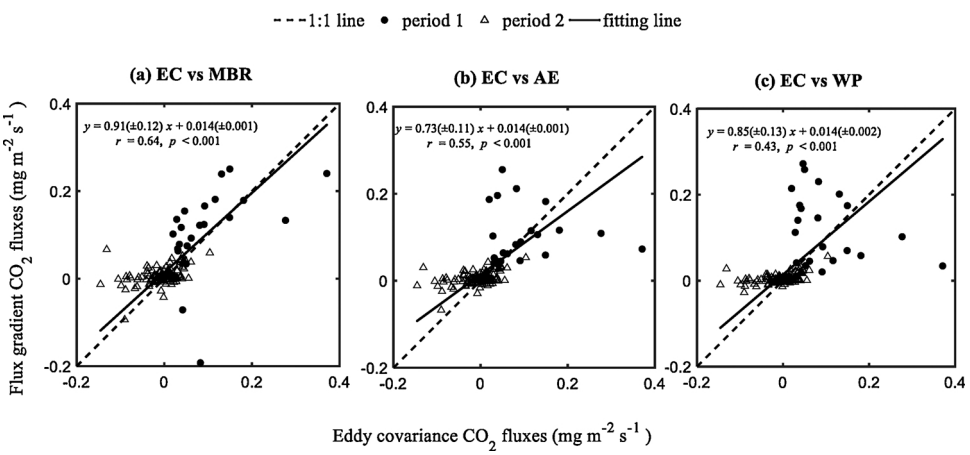

Fig. 4. Same as in Fig. 3 but for CO_2 flux.

effect (Section 3.4).

The WP K was highly correlated with the AE K, indicating that wind speed was a more important factor than air stability in controlling eddy diffusion efficiency. The WP K was biased low in unstable conditions for both measurement periods and in neutral conditions for Period 1. The low biases in unstable conditions is consistent with fact that the WP method did not involve the stability correction factor φ_h which is less than unity in unstable conditions. In principle, the WP and AE should yield nearly identical K values for neutral stability according to Eqs. (2) and (5). Indeed the two methods were in good agreement for Period 2 (Fig. 6b). But the fact that they did not agree for Period 1 indicates that the surface roughness (z_o = 0.078 m) used here was too low. This surface roughness was determined by linear regression of the friction velocity u_* against the mean wind speed u measured over the whole dry season in 2016 (March 1 to May 1) when there was no water in Ponds D and F, which was much longer than the FG measurement Period 1 (March24–31).

3.4. Impact of footprint

The flux footprint of the EC system was larger than that of the FG system due to the higher observation height (Fig. 7). According to the model of Kljun et al. (2015), the source contribution from the two targeted ponds was roughly 81% and 85% for the EC and FG fluxes, respectively, during Period 1. The contribution was increased to 84% for the EC flux and 88% for the FG flux during Period 2 due to the lower measurement heights, even though the surface roughness in Period 2 was smaller than in Period 1.

The one-dimensional cumulative footprints calculated with the Horst (1999) model for Period 2 (Fig. 8) were broadly consistent with the two-dimensional results shown in Fig. 7. Here, the direct EC footprint was computed for the EC measurement height of 2.0 m, the profile footprint from the finite difference relationship (Eq. (16) of Horst, 1999) for heights z_1 = 0.9 m and z_2 = 2.2 m, and the gradient footprint for the geometric mean height of z_1 and z_2 (=1.4 m). At the prevailing wind direction (NE, Fig. 7), the fetch distance was about 120 m. At this fetch distance the cumulative source contribution was 73% for the direct EC measurement and 82% for the gradient measurement. Additionally, Horst (1999) predicts that the source footprint, or "profile footprint", should be smaller for the flux determined with the two-level profile measurement than the footprint, or "gradient footprint", for the gradient flux measured at the geometric mean height of the two inlets. (If the direct EC footprint was computed for the geometric mean height of 1.4 m, it would be nearly identical the gradient footprint shown in Fig. 8 according to Horst, 1999). Our calculations were consistent with this prediction. At the same fetch distance of 120 m, the cumulative

Table 2
Average eddy diffusivity (m^{-2} s^{-1}) (± one standard deviation) calculated using three eddy diffusivity models during the different observation periods.

Observation Period	AE	MBR	WP
Period 1	0.131 (± 0.100)	0.187 (± 0.172)	0.110 (± 0.062)
Period 2	0.143 (± 0.039)	0.178 (± 0.077)	0.098 (± 0.043)
Total	0.140 (± 0.059)	0.180 (± 0.106)	0.101 (± 0.048)

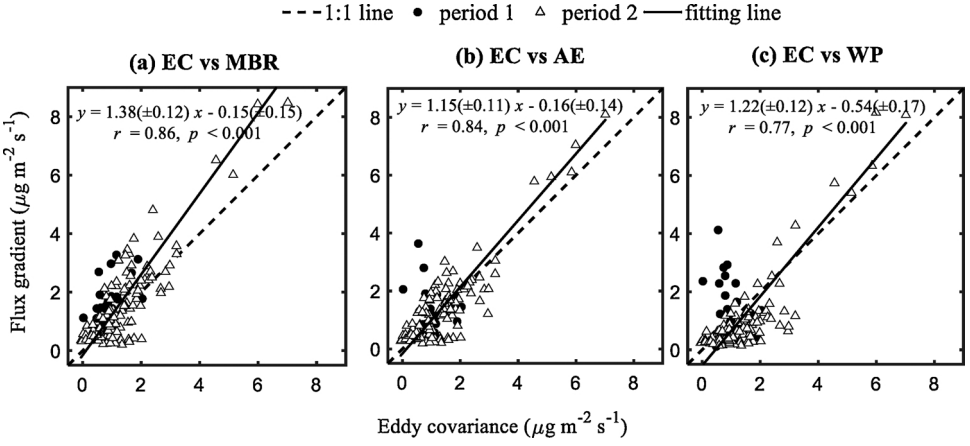

Fig. 5. Same as Fig. 3 but for CH_4 flux.

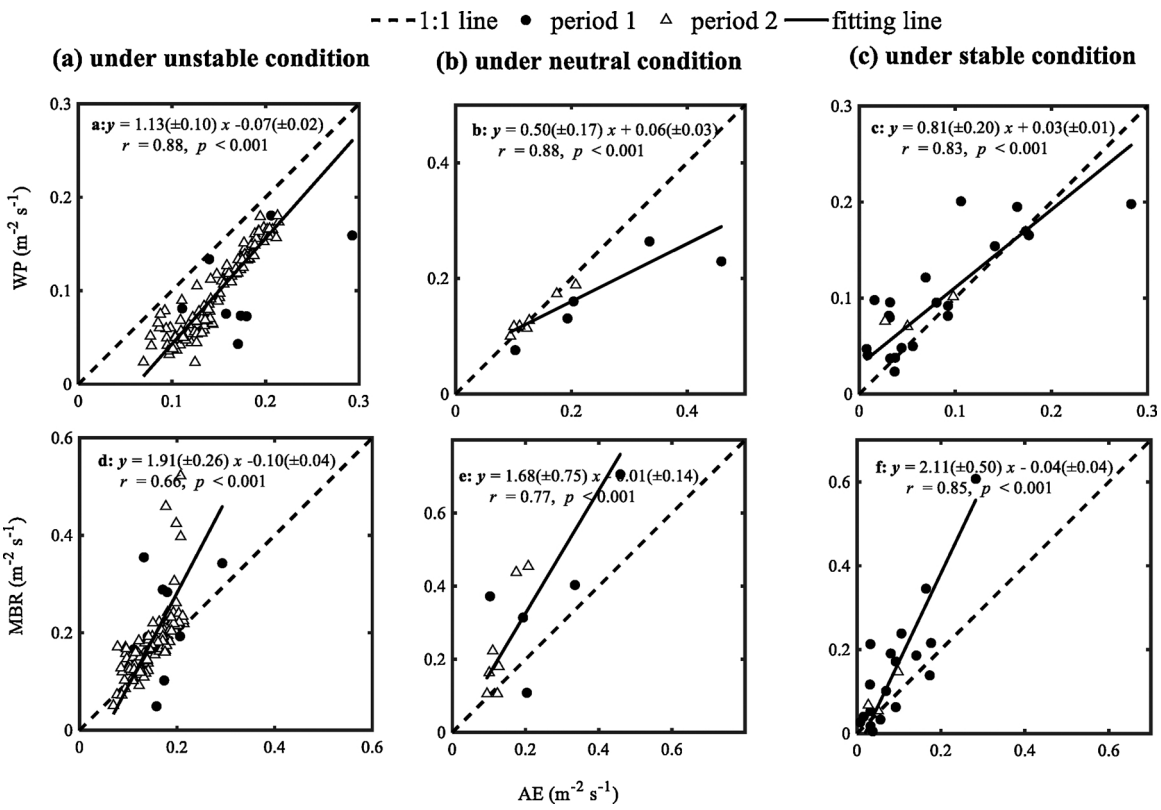

Fig. 6. Comparison of eddy diffusivity calculated among three methods (AE – aerodynamic method, WP – wind profile, and MBR – modified Bowen ratio) during the different stability conditions. Also shown are regression equation, linear correlation (*r*) and significance (*p*). Parameter bounds on the regression coefficients are 95% confidence intervals.

contribution to the two-level profile flux was 88%. The peak contribution to the two-level profile flux occurred at a distance of 14 m, whereas the peak contribution to the eddy covariance flux occurred further away, at a distance of 25 m.

Our study appears to provide the first experimental confirmation of Horst's prediction that the footprint of the two-level profile flux should be smaller than the footprint of the gradient flux or the footprint of the direct eddy covariance flux. The AE method yielded a stable and persistently positive CO_2 flux for Period 2 (Supplementary Fig. S3) when the two target ponds were filled with water, at a magnitude expected of water bodies free of photosynthetic activities (Xiao et al., 2014b; Holgerson and Raymond, 2016). But the EC CO_2 flux displayed a strong diurnal pattern with slightly positive values at night and more negative values during the day. A logical interpretation is that the AE flux footprint was even smaller than predicted by the Horst model, to the extent that it fell within the boundary of the two target ponds and therefore the AE flux represented their true source strength. In contrast, because the EC flux footprint extended beyond the boundary of the ponds, it was contaminated by photosynthesis in the day and respiration at night of the plants surrounding the ponds. Because these plant fluxes were one to two orders of magnitude larger than the true flux of the target ponds, even a slight footprint contamination could cause large relative errors.

To support the above interpretation, we performed a simple two-source flux calculation. The CO_2 flux measured with the EC method consists of two components as

$$F = F_1 f + F_2 (1 - f) \quad (7)$$

where F_1 is the true CO_2 flux of the two target ponds (taken here as 0.006 mg m^{-2} s^{-1}), F_2 is the true flux from sources outside the boundary of these two ponds, and f is the footprint contribution from the two ponds calculated by the Kljun model (2015). No CO_2 flux measurement was made of the upland systems near the ponds. The eddy covariance observation at a land site about 200 km to the east of our site (the Dongshan site, Lee et al. 2014) yielded a CO_2 flux about -20 μmol m^{-2} s^{-1} under full sunlight (solar radiation 700 W m^{-2}) in the daytime and about 7 μmol m^{-2} s^{-1} at night, in late September to early October 2018. The landscape at that site was similar to that surrounding the fish ponds (cropland with scattered fish ponds and small villages). So F_2 was parameterized as F_2 = 0.31 mg m^{-2} s^{-1} at night and F_2 = -0.9 (S / 700) mg m^{-2} s^{-1} during the day, where S is incoming solar radiation in W m^{-2}. This simple two-source calculation captured the broad temporal patterns seen in the EC flux (Fig. 9).

The larger relative difference between the EC and AE latent heat flux observed during Period 1 (43%) than during Period 2 (17%) can also be interpreted in the footprint context. In Period 1, the target ponds were dry, whereas the surrounding land patches (lotus Pond B, wet Ponds A, C and E, and rice paddies to the northeast of Ponds D and F; Fig. 1) were generally wet, resulting in large contrasts in the local evaporation rate. The relatively high EC latent heat flux (compared to the AE latent flux) in Period 1 was a result of evaporative contributions from sources situated outside the dry ponds. The landscape variability was much reduced in Period 2 when the target ponds were filled with water, and the two methods achieved better agreement than in Period 1.

Of the three gas fluxes investigated, the CH_4 flux appeared least prone to surface source heterogeneity, as indicated by the overall good agreement between the AE and the EC data (Fig. 5b; Table 1). Even though the CH_4 source fractional contributions were the same as those of H_2O and CO_2, it appears that the strength of the CH_4 sources outside the two target ponds was similar in magnitude to the source strength of these ponds.

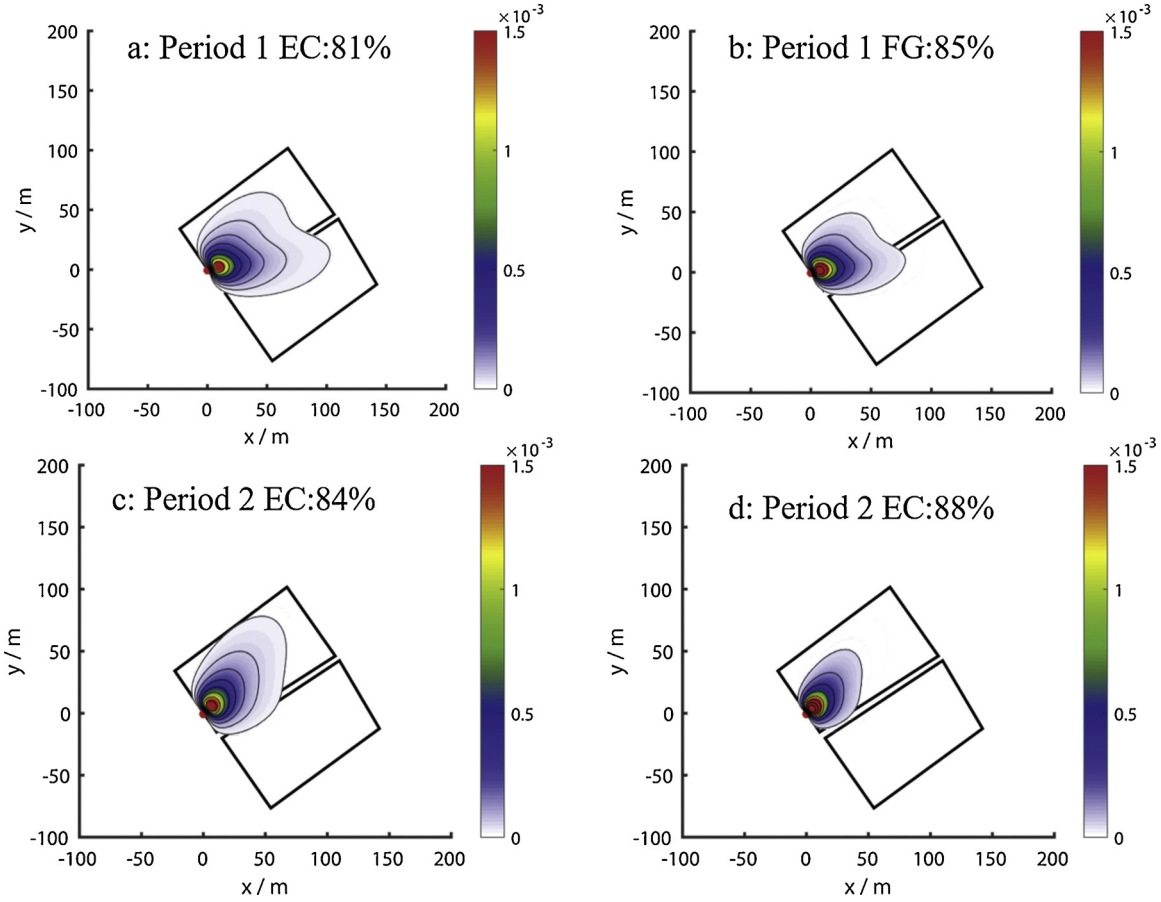

Fig. 7. Flux footprint for the EC and the FG system according to the footprint model of Kljun et al. (2015). Footprint contour lines are shown in intervals of 10% from 10% to 80%. The percent value in each panel is the source contribution from the two target ponds.

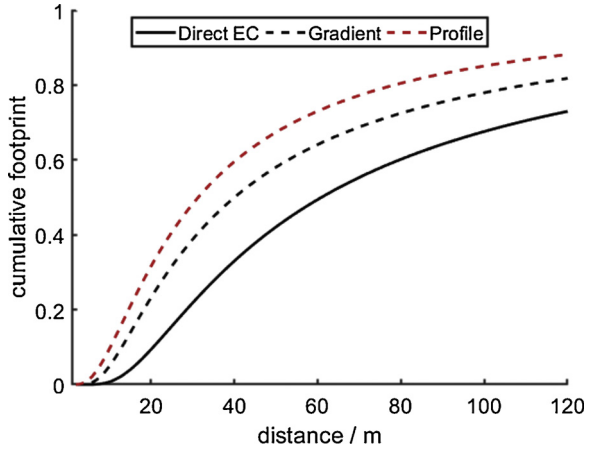

Fig. 8. One-dimensional cumulative footprints according to the Horst (1999) model.

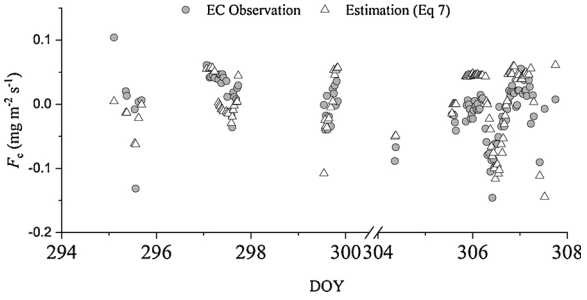

Fig. 9. Time series of CO_2 flux obtained by EC observation and two-source footprint estimation (Eq. (7)).

3.5. Published results on methods comparison

Previous comparison studies on the AE and the EC methods for measuring trace gas fluxes have shown variable results. Good agreement between the two methods has been reported for a peatland (Karlsson, 2017) and a sub-alpine grassland (Fritsche et al., 2008). Common to these studies are large concentration gradients in the surface layer and high precision of the instruments used for measuring the trace gas gradients. However, large scatters have been reported in some studies, including studies at a pasture (Laubach et al., 2016) and at a forest (Wu et al., 2015), and the likely explanation was large uncertainties in the concentration gradient measurement, leading to larger scatters in the AE fluxes, especially under conditions of small concentration gradients.

It is well known that the turbulent Schmidt number (Sc), or the ratio eddy diffusivity for momentum to the diffusivity for scalars, is less than unity in unstable conditions. The AE model accounted for this difference because it deployed the stability correction function for heat, not for momentum. However, it assumed that Sc is equal to one under neutral stability, an assumption that has been challenged by several observational studies. In the roughness sublayer above vegetation stands, the coherence eddies generated by inflection point instability are more efficient in transporting scalars than momentum, resulting in Sc smaller than unity: The Sc values reported by Simpson et al. (1998) for a deciduous forest vary in the range of 0.64 to 0.85 in neutral conditions, and are in broad agreement with the values found for

another forest (Denmead and Bradley, 1985). More recently, Wilson (2013) reported that the mean Sc for water vapor and carbon dioxide is 0.68 and 0.78, respectively, above a spring wheat crop during near-neutral stratification. On the other hand, with a few exceptions (e.g., Flesch et al., 2002), the general view is that for the lack of the inflection-point instability, Sc = 1 is a good approximation over smooth surfaces including water bodies and bare soils (Kaimal and Finnigan, 1994).

It is a common practice to use H_2O as the tracer for the MBR method. Excellent agreement between the MBR and the AE CH_4 flux was reported for an extensive rice paddy (Simpson et al., 1995). Xiao et al. (2014b) compared the CO_2 and CH_4 obtained using the MBR method and the AE method over a large lake and found excellent agreement between the two methods. A similar conclusion can be inferred from Griffith et al. (2002) who deployed the MBR method to measure the CO_2, CH_4, and N_2O fluxes over a pasture land. Although they did not compare the eddy diffusivity, they found very good agreement between the MBR and the EC CO_2 flux. These studies indicate that, for extensive and homogeneous surfaces, the eddy diffusivity for H_2O follows the AE parameterization.

The assumption made by the MBR method, that eddy diffusivity is invariant among the target gas species and the scalar used as the tracer, is valid only if these gases and the tracer have similar spatial distributions of their source or sink locations (Wolf et al., 2008; Meredith et al., 2014; Laubach et al., 2016). Wolf et al. (2008) reported large differences in the CO_2 flux over a shortgrass ecosystem between the MBR and the EC method. In their study, the MBR eddy diffusivity was calculated from the vertical temperature gradient, and may not apply to CO_2 due to the low correlation between CO_2 and temperature, especially under neutral conditions. In an MBR versus EC comparative study over a forest, Meredith et al. (2014) deployed H_2O as the tracer to measure CO_2 as the target gas. They found that the eddy diffusivity for H_2O was 32% lower than the eddy diffusivity for CO_2, which violates the basic assumption of the MBR method. In their study, the discrepancy arises from different distributions of sources and sinks between CO_2 and H_2O in the vertical direction: besides canopy sources and sinks, CO_2 has a stronger source from the soil than H_2O. On the other hand, in an experiment on CH_4 flux in a rice paddy, Simpson et al. (1995) reported excellent agreement (to within 1%) between the MBR and the AE method. Their success can be attributed to the fact that in their extensive and flooded rice field, both the measurement target (CH_4) and the tracer (H_2O) had similar source distributions in the vertical and the horizontal directions. In the present study, the lack of agreement between the MBR and the EC trace gas fluxes (Table 1) can be explained by differences in horizontal source distributions between the tracer scalar (H_2O) and the target gases (CH_4 and CO_2; Section 3.4). Consistent with the published results, our findings argue against using the MBR method in a landscape where the source and sink distributions of the target gas and the tracer are highly heterogenous.

4. Conclusions

In this paper, we evaluated the eddy covariance (EC) method and three eddy diffusivity models [aerodynamic model (AE), modified Bowen-ratio model (MBR), and wind profile model (WP)] for use with the flux-gradient (FG) method for measuring the CO_2, CH_4, and H_2O fluxes from two small fish ponds. We found that the EC flux errors due to high frequency loss were on average 18%, 8% and 14% for the CH_4, the water vapor, and the CO_2 flux, respectively. After the frequency loss correction using the algorithm imbedded in the EddyPro software, the EC fluxes were in better agreement with the fluxes measured with the AE method.

Our study supports Horst's (1999) prediction that the flux obtained by the AE method should have a much smaller footprint than the flux measured by the EC method. The CO_2 flux measured with the AE method for Period 2 was slightly positive (0.006 ± 0.001 mg m^{-2} s^{-1}), at a magnitude typical of inland water bodies. On the other hand, the EC CO_2 flux displayed a strong diurnal variation of positive values at night (about 0.012 mg m^{-2} s^{-1}) and negative values during the day (as negative as -0.15 mg m^{-2} s^{-1}), indicating large contamination by sources outside the boundary of the target ponds.

Of the three eddy diffusivity models, the MBR model yielded the largest CH_4 flux (1.66 μg m^{-2} s^{-1}, mean of the two periods), the WP yielded the smallest flux (1.05 μg m^{-2} s^{-1}), and the AE flux was in between (1.34 μg m^{-2} s^{-1}). For comparison, the mean EC CH_4 flux was 1.31 μg m^{-2} s^{-1}. The high bias with the MBR model was attributed to the fact that the H_2O flux measured by the EC method was influenced by stronger H_2O sources outside the fish ponds, especially in Period 1. The WP model did not perform well due to the omission of the influence of atmospheric stability on eddy diffusion.

In summary, the FG method using the AE model appears best suited for measuring fluxes from small ponds. This is a hybrid scheme whereby an EC system is used to measure the friction velocity and the sensible heat flux, two parameters needed for calculating the eddy diffusivity, and a precision gas analyzer is used to measure the concentration of the target gas at two heights very close to the surface.

Acknowledgements

This research was supported by the National Natural Science Foundation of China (grant numbers 41575147, 41801093, and 41475141) and the Priority Academic Program Development of Jiangsu Higher Education Institutions (grand number PAPD). We thank students in the Yale-NUIST Center on Atmospheric Environmental for their assistance with the field experiment.

Appendix A. Supplementary data

Supplementary material related to this article can be found, in the online version, at doi:https://doi.org/10.1016/j.agrformet.2019.05.032.

References

Abnizova, A., Siemens, J., Langer, M., Boike, J., 2012. Small ponds with major impact: the relevance of ponds and lakes in permafrost landscapes to carbon dioxide emissions. Global Biogeochem. Cycles 26, GB2041.
Baldocchi, D.D., Hicks, B.B., Meyers, T.P., 1988. Measuring biosphere-atmosphere exchanges of biologically related gases with micrometeorological methods. Ecology 69 (5), 1331–1340.
Businger, J., 1986. Evaluation of the accuracy with which dry deposition can be measured with current micrometeorological techniques. J. Clim. Appl. Meteorol. 25 (8), 1100–1124.
Catalán, N., von Schiller, D., Marcé, R., Koschorreck, M., Gomez-Gener, L., Obrador, B., 2014. Carbon dioxide efflux during the flooding phase of temporary ponds. Limnetica 33 (2), 349–360.
Cole, J.J., Caraco, N.F., 1998. Atmospheric exchange of carbon dioxide in a low-wind oligotrophic lake measured by the addition of SF_6. Limnol. Oceanogr. 43 (4), 647–656.
Cole, J.J., Bade, D.L., Bastviken, D., Pace, M.L., Van de Bogert, M., 2010. Multiple approaches to estimating air-water gas exchange in small lakes. Limnol. Oceanogr. Methods 8 (6), 285–293.
DelSontro, T., Boutet, L., St-Pierre, A., del Giorgio, P.A., Prairie, Y.T., 2016. Methane ebullition and diffusion from northern ponds and lakes regulated by the interaction between temperature and system productivity. Limnol. Oceanogr. 61, S62–S77.
Denmead, O.T., Bradley, E.F., 1985. Flux-gradient relationships in a forest canopy. The Forest-atmosphere Interaction. Springer, Dordrecht, pp. 421–442.
Downing, J.A., Prairie, Y.T., Cole, J.J., Duarte, C.M., Tranvik, L.J., Striegl, R.G., Middelburg, J.J., 2006. The global abundance and size distribution of lakes, ponds, and impoundments. Limnol. Oceanogr. 51 (5), 2388–2397.
Dyer, A.J., Hicks, B.B., 1970. Flux-gradient relationships in the constant flux layer. Q. J. R. Meteorol. Soc. 96 (410), 715–721.
Flesch, T.K., Prueger, J.H., Hatfield, J.L., 2002. Turbulent Schmidt number from a tracer experiment. Agric. For. Meteorol. 111 (4), 299–307.
Griffith, D.W.T., Leuning, R., Denmead, O.T., Jamie, I.M., 2002. Air–land exchanges of CO_2, CH_4 and N_2O measured by FTIR spectrometry and micrometeorological techniques. Atmos. Environ. 36 (11), 1833–1842.
Helbig, M., Wischnewski, K., Gosselin, G.H., Biraud, S.C., Bogoev, I., Chan, W.S., Euskirchen, E.S., Glenn, A.J., Marsh, P.M., Quinton, W.L., Sonnentag, O., 2016. Addressing a systematic bias in carbon dioxide flux measurements with the EC150

and the IRGASON open-path gas analyzers. Agric. For. Meteorol. 228, 349–359.
Holgerson, M.A., 2015. Drivers of carbon dioxide and methane supersaturation in small, temporary ponds. Biogeochemistry 124 (1-3), 305–318.
Holgerson, M.A., Raymond, P.A., 2016. Large contribution to inland water CO_2 and CH emissions from very small ponds. Nat. Geosci. 9 (3), 222–226.
Horst, T.W., 1999. The footprint for estimation of atmosphere-surface exchange fluxes by profile techniques. Bound. Layer Meteorol. 90 (2), 171–188.
Hu, Z., Lee, J.W., Chandran, K., Kim, S., Khanal, S.K., 2012. Nitrous oxide (N_2O) emission from aquaculture: a review. Environ. Sci. Technol. 46 (12), 6470–6480.
Huttunen, J.T., Alm, J., Liikanen, A., Juutinen, S., Larmola, T., Hammar, T., Martikainen, P.J., 2003. Fluxes of methane, carbon dioxide and nitrous oxide in boreal lakes and potential anthropogenic effects on the aquatic greenhouse gas emissions. Chemosphere 52 (3), 609–621.
Jonsson, A., Åberg, J., Lindroth, A., Jansson, M., 2008. Gas transfer rate and CO_2 flux between an unproductive lake and the atmosphere in northern Sweden. J. Geophys. Res. 113, G04006.
Kaimal, J.C., Wyngaard, J.C.J., Izumi, Y., Coté, O.R., 1972. Spectral characteristics of surface-layer turbulence. Q. J. R. Meteorol. Soc. 98 (417), 563–589.
Kaimal, J.C., Finnigan, J.J., 1994. Atmospheric Boundary Layer Flows: Their Structure and Measurement. Oxford University Press.
Karlsson, K., 2017. Greenhouse Gas Flux at a Temperate Peatland: a Comparison of the Eddy Covariance Method and the Flux-Gradient Method. Student Thesis Series. INES.
Kljun, N., Calanca, P., Rotach, M.W., Schmid, H.P., 2015. A simple two-dimensional parameterisation for Flux Footprint Prediction (FFP). Geosci. Model. Dev. 8 (11), 3695–3713.
Kormann, R., Meixner, F.X., 2001. An analytical footprint model for non-neutral stratification. Bound. Layer Meteorol. 99 (2), 207–224.
Fritsche, J., Obrist, D., Zeeman, M.J., Conen, F., Eugster, W., Alewell, C., 2008. Elemental mercury fluxes over a sub-alpine grassland determined with two micrometeorological methods. Atmos. Environ. 42 (13), 2922–2933.
Laubach, J., Barthel, M., Fraser, A., Hunt, J.E., Griffith, D.W., 2016. Combining two complementary micrometeorological methods to measure CH_4 and N_2O fluxes over pasture. Biogeosciences 13, 1309–1327.
Lee, X., Massman, W., Law, B. (Eds.), 2004. Handbook of Micrometeorology: a Guide for Surface Flux Measurement and Analysis Vol. 29 Springer Science & Business Media.
Lee, X., Liu, S., Xiao, W., Wang, W., Gao, Z., Cao, C., Wen, X., 2014. The Taihu Eddy Flux Network: an observational program on energy, water, and greenhouse gas fluxes of a large freshwater lake. Bull. Am. Meteorol. Soc. 95 (10), 1583–1594.
Lee, X., 2018. Fundamentals of Boundary-Layer Meteorology. Springer, Berlin.
Liu, S., Hu, Z., Wu, S., Li, S., Li, Z., Zou, J., 2015. Methane and nitrous oxide emissions reduced following conversion of rice paddies to inland crab–fish aquaculture in Southeast China. Environ. Sci. Technol. 50 (2), 633–642.
McDermitt, D., Burba, G., Xu, L., Anderson, T., Komissarov, A., Riensche, B., Schedlbauer, J., Starr, G., Zona, D., Oechel, W., Oberbauer, S., Hastings, S., 2011. A new low-power, open-path instrument for measuring methane flux by eddy covariance. Appl. Phys. B 102 (2), 391–405.
Meredith, L.K., Commane, R., Munger, J.W., Dunn, A., Tang, J., Wofsy, S.C., Prinn, R.G., 2014. Ecosystem fluxes of hydrogen: a comparison of flux-gradient methods. Atmos. Meas. Tech. 7, 2787–2805.
Meyers, T.P., Hall, M.E., Lindberg, S.E., Kim, K.I., 1996. Use of the modified Bowen-ratio technique to measure fluxes of trace gases. Atmos. Environ. 30 (19), 3321–3329.
Moncrieff, J.B., Massheder, J.M., De Bruin, H., Elbers, J., Friborg, T., Heusinkveld, B., Kabat, P., Scott, S., Søgaard, H., Verhoef, A., 1997. A system to measure surface fluxes of momentum, sensible heat, water vapour and carbon dioxide. J. Hydrol. 188, 589–611.
Monteith, J.L., Szeicz, G., 1960. The carbon-dioxide flux over a field of sugar beet. Q. J. R. Meteorol. Soc. 86 (368), 205–214.
Monteith, J.L., Unsworth, M.H., 1990. Principles of Environmental Biophysics, 2nd edition. Edward Arnold, London 291pp.
Moore, C.J., 1986. Frequency response corrections for eddy correlation systems. Bound. Layer Meteorol. 37 (1-2), 17–35.
Natchimuthu, S., Selvam, B.P., Bastviken, D., 2014. Influence of weather variables on methane and carbon dioxide flux from a shallow pond. Biogeochemistry 119 (1-3), 403–413.
Schubert, C.J., Diem, T., Eugster, W., 2012. Methane emissions from a small wind shielded lake determined by eddy covariance, flux chambers, anchored funnels, and boundary model calculations: a comparison. Environ. Sci. Technol. 46 (8), 4515–4522.
Simpson, I.J., Thurtell, G.W., Kidd, G.E., Lin, M., Demetriades-Shah, T.H., Flitcroft, I.D., Neue, H.U., 1995. Tunable diode laser measurements of methane fluxes from an irrigated rice paddy field in the Philippines. J. Geophys. Res. Atmos. 100 (D4), 7283–7290.
Simpson, I.J., Thurtell, G.W., Neumann, H.H., Den Hartog, G., Edwards, G.C., 1998. The validity of similarity theory in the roughness sublayer above forests. Bound. Layer Meteorol. 87 (1), 69–99.
Swinbank, W.C., 1951. The measurement of vertical transfer of heat and water vapor by eddies in the lower atmosphere. J. Meteorol. 8 (3), 135–145.
Tanner, C.B., Thurtell, G.W., 1969. Anemoclinometer Measurements of Reynolds Stress and Heat Transport in the Atmospheric Surface Layer. Wisconsin Univ-Madison Dept of Soil Science.
Verpoorter, C., Kutser, T., Seekell, D.A., Tranvik, L.J., 2014. A global inventory of lakes based on high-resolution satellite imagery. Geophys. Res. Lett. 41, 6396–6402.
Webb, E.K., Pearman, G.I., Leuning, R., 1980. Correction of flux measurements for density effects due to heat and water vapour transfer. Q. J. R. Meteorol. Soc. 106 (447), 85–100.
Wik, M., Varner, R.K., Anthony, K.W., MacIntyre, S., Bastviken, D., 2016. Climate-sensitive northern lakes and ponds are critical components of methane release. Nat. Geosci. 9 (2), 99.
Williams, J., Crutzen, P.J., 2010. Nitrous oxide from aquaculture. Nat. Geosci. 3 (3), 143.
Wilson, J.D., 2013. Turbulent Schmidt numbers above a wheat crop. Boundary. Layer Meteorol. 148 (2), 255–268.
Wolf, A., Saliendra, N., Akshalov, K., Johnson, D.A., Laca, E., 2008. Effects of different eddy covariance correction schemes on energy balance closure and comparisons with the modified Bowen ratio system. Agric. For. Meteorol. 148 (6-7), 942–952.
Wu, Z.Y., Zhang, L., Wang, X.M., Munger, J.W., 2015. A modified micrometeorological gradient method for estimating O_3 dry depositions over a forest canopy. Atmos. Chem. Phys. 15 (13), 7487–7496.
Xiao, S., Yang, H., Liu, D., Zhang, C., Lei, D., Wang, Y., Wu, G., 2014a. Gas transfer velocities of methane and carbon dioxide in a subtropical shallow pond. Tellus B Chem. Phys. Meteorol. 66 (1), 23795.
Xiao, W., Liu, S., Li, H., Xiao, Q., Wang, W., Hu, Z., Zhang, M., 2014b. A Flux-gradient system for simultaneous measurement of the CH_4, CO_2, and H_2O fluxes at a lake–air interface. Environ. Sci. Technol. 48 (24), 14490–14498.
Yuan, J., Xiang, J., Liu, D., Kang, H., He, T., Kim, S., Ding, W., 2019. Rapid growth in greenhouse gas emissions from the adoption of industrial-scale aquaculture. Nat. Clim. Chang. 9, 318–322.
Zappa, C.J., Raymond, P.A., Terray, E.A., McGillis, W.R., 2003. Variation in surface turbulence and the gas transfer velocity over a tidal cycle in a macro-tidal estuary. Estuaries 26 (6), 1401–1415.